Received: 3 February 2020 | Revised: 1 May 2020 | Accepted: 17 May 2020

DOI: 10.1111/mmi.14532

Check for updates

WILEY

RESEARCH ARTICLE

Calcium homeostasis plays important roles in the internalization and activities of the small synthetic antifungal peptide PAF26

Akira J. T. Alexander [1] | Alberto Muñoz [2] | Jose F. Marcos [3] | Nick D. Read [4]

[1]Institute of Infection, Immunity & Inflammation, The University of Glasgow, Glasgow, Scotland

[2]MRC Centre for Medical Mycology, University of Exeter, Exeter, UK

[3]Department of Food Biotechnology, Instituto de Agroquímica y Tecnología de Alimentos (IATA) , Consejo Superior de Investigaciones Científicas (CSIC), Valencia, Spain

[4]Manchester Fungal Infection Group, Infection, Immunity & Respiratory Medicine, University of Manchester, Manchester, UK

Correspondence
Akira J. T. Alexander, Institute of Infection, Immunity & Inflammation, The University of Glasgow, 464 Bearsden Rd, Bearsden, Glasgow, G61 1QH, Scotland.
Email: akira.alexander@glasgow.ac.uk

Funding information
Funding for this project was provided by a Biotechnology and Biological Sciences Research Council Research Studentship to AJTA. The funders had no role in study design, data collection and analysis, decision to publish, or preparation of the manuscript.

Abstract

Fungal diseases are responsible for the deaths of over 1.5 million people worldwide annually. Antifungal peptides represent a useful source of antifungals with novel mechanisms-of-action, and potentially provide new methods of overcoming resistance. Here we investigate the mode-of-action of the small, rationally designed synthetic antifungal peptide PAF26 using the model fungus *Neurospora crassa*. Here we show that the cell killing activity of PAF26 is dependent on extracellular Ca^{2+} and the presence of fully functioning fungal Ca^{2+} homeostatic/signaling machinery. In a screen of mutants with deletions in Ca^{2+}-signaling machinery, we identified three mutants more tolerant to PAF26. The Ca^{2+} ATPase NCA-2 was found to be involved in the initial interaction of PAF26 with the cell envelope. The vacuolar Ca^{2+} channel YVC-1 was shown to be essential for its accumulation and concentration within the vacuolar system. The Ca^{2+} channel CCH-1 was found to be required to prevent the translocation of PAF26 across the plasma membrane. In the wild type, Ca^{2+} removal from the medium resulted in the peptide remaining trapped in small vesicles as in the *Δyvc-1* mutant. It is, therefore, apparent that cell killing by PAF26 is complex and unusually dependent on extracellular Ca^{2+} and components of the Ca^{2+}-regulatory machinery.

KEYWORDS

antifungal peptides, antimicrobial agents , calcium signalling , mechanisms of action, PAF26, resistance

1 | INTRODUCTION

Fungal infections today are among the most difficult diseases to manage in humans (Kohler *et al*., 2014). Fungi collectively kill over 1.5 million people annually which is more than malaria and similar to the death toll from tuberculosis (Brown *et al*., 2012; Bongomin *et al*., 2017). Increasing resistance to the limited arsenal of antifungal drugs is a serious concern, especially for *Candida* and *Aspergillus* infections, for which the therapeutic options are limited. Overall, there is an urgent need to develop new antifungal strategies to tackle fungal infections (Denning and Bromley, 2015; Nicola *et al*., 2019).

In loving memory of our colleague, mentor, and above all, dear friend Professor Nick D. Read. He never stopped caring, advising and providing help to those in need.

This is an open access article under the terms of the Creative Commons Attribution License, which permits use, distribution and reproduction in any medium, provided the original work is properly cited.
© 2020 The Authors. Molecular Microbiology published by John Wiley & Sons Ltd

Antifungal peptides (AFPs) and peptide-related molecules are being intensively studied as alternatives for the therapeutic control of pathogenic fungi (Matejuk *et al*., 2010; Duncan and O'Neil, 2013; Rautenbach *et al*., 2016; Nicola *et al*., 2019). A detailed understanding of their antimicrobial mechanisms is of high priority if peptides are to be considered as useful antifungal agents. These studies may also aid the identification of novel targets for antifungal therapy (Muñoz *et al*., 2013a; Rautenbach *et al*., 2016). Furthermore, this mechanistic understanding is guiding the de novo design and modification of natural peptides in order to circumvent their limitations (e.g., instability, toxicity, interactions with other drugs, poor kinetics, resistance mechanisms, etc) and thus improve their antimicrobial efficacy (Nicola *et al*., 2019). Overall, AFPs offer promising alternatives to standard therapies as anti-infectives and immunomodulatory agents with mechanisms-of-action less prone to resistance induction compared to conventional antibiotics (Mahlapuu *et al*., 2016).

PAF26 is a synthetic hexapeptide that has been shown to be highly effective at killing filamentous fungi while showing low toxicity against human and bacterial cells (Munoz *et al*., 2006). Unlike membrane permeabilizing antimicrobials, initial investigations into the mode-of-action of PAF26 indicated that it did not directly permeabilize the plasma membrane. Instead, at low fungicidal concentrations, PAF26 has a dynamic antifungal mechanism-of-action that involves at least three stages: peptide interaction with the fungal cell envelope (cell wall and/or plasma membrane), endocytic internalization and accumulation in the vacuole followed by vacuolar expansion. At a certain point, PAF26 is actively transported out of the vacuole into the cytoplasm, followed by a series of complex and specific intracellular effects whose relationship with the eventual death of the target fungus is still unclear (Muñoz *et al*., 2012). Two functional and separate motifs (cationic and hydrophobic domains) in the peptide amino acid sequence have been identified as playing important roles in the antimicrobial mode-of-action (Muñoz *et al*., 2013). As a result of these studies, PAF26 has been proposed as a simple peptide model for the characterization and study of cationic, cell-penetrating AFPs (Muñoz *et al*., 2012; 2013a).

From average measurements of fungal cell populations expressing the genetically encoded Ca^{2+}-reporter aequorin, cytosolic free Ca^{2+} concentrations ($[Ca^{2+}]_{cyt}$) within *Neurospora crassa* spore germlings treated with a low inhibitory concentration of PAF26 (2.5-5 μM) have been shown to exhibit a biphasic increase in response to PAF26, and this biphasic $[Ca^{2+}]_{cyt}$ increase is completely dependent on the PAF26 and extracellular Ca^{2+} concentrations. The second phase of the biphasic $[Ca^{2+}]_{cyt}$ increase was found to be energy dependent because it was blocked by treatment with the metabolic inhibitor, sodium azide (NaN_3). This may link PAF26 internalization with actin-dependent endocytosis. Consistent with endocytic internalization playing a key role in PAF26 internalization, is the inhibition by the F-actin inhibitor, Latrucunulin A and a reduced uptake rate in endocytosis by the endocytic mutants *Δrvs-167*, *Δrvs-161*, and *Δrab-5* (Muñoz *et al*., 2012; 2013a). At high fungicidal concentrations (15 μM), PAF26 killed cells even after NaN_3 treatment, although in a different manner. Under these conditions, the peptide first bound to the cell envelope as before, but was then observed to directly enter the cytoplasm, indicating passive transport across the plasma membrane at high concentrations (Muñoz *et al*., 2012).

In the current research, evidence for Ca^{2+}-signaling having a significant role in the PAF26 mode-of-action was analyzed by testing and analyzing the PAF26 sensitivity of deletion mutants defective in different components of their Ca^{2+}-signaling machinery. The pattern and kinetics of peptide interaction, internalization and distribution within the cells of PAF26-resistant mutants were compared with the parental wild type using fluorescently labeled PAF26 combined with live-cell imaging. The role of external Ca^{2+} in these processes and vacuolar fusion was assessed.

2 | RESULTS

2.1 | Sensitivity of fungal cells to killing by PAF26 is dependent on extracellular Ca^{2+}

To confirm that extracellular Ca^{2+} plays a role in determining the sensitivity of *N. crassa* to PAF26 (Muñoz *et al*., 2012), and thus Ca^{2+} homeostasis being involved in the mode-of-action of PAF26; the wild-type strain was grown in: (a) standard Vögels medium (VM) (0.64 mM Ca^{2+}); (b) Ca^{2+} free VM (in which Ca^{2+} had been omitted); and (c) VM with twice the normal concentration of Ca^{2+} (1.28 mM). The IC_{50} values for the wild type under these different media are shown in Figure 1a. The IC_{50} in standard VM was 3.7 ± 0.6 μM and in VM lacking Ca^{2+} was 6.4 ± 0.9 μM, a significant increase in resistance against PAF26 ($p \leq .001$). VM with 2 X Ca^{2+} had an IC_{50} value of 2.5 ± 0.4 μM, a significant increase in sensitivity to PAF26 ($p \leq .01$) compared with standard VM. These results are consistent with a Ca^{2+}-dependent mechanism playing a role in determining the sensitivity of *N. crassa* to PAF26 involving uptake of Ca^{2+} from the external medium.

2.2 | PAF26 requires a functional $[Ca^{2+}]_{cyt}$ homeostatic machinery in order to kill fungal cells

To assess whether Ca^{2+}-homeostasis and signaling play a role in the mode-of-action of PAF26; 24 homokaryotic deletion mutants of genes encoding proteins predicted to be components of the *N. crassa* Ca^{2+}-homeostatic machinery were screened for increased PAF26 tolerance/ sensitivity. The predicted locations of these proteins in the fungal cell are shown in Figure 1c; The results of the screen are in Table 1.

The first group of mutants screened were defective in the following Ca^{2+}-channel proteins: CCH-1 and MID-1, which are components of the high affinity Ca^{2+}-influx system (HACS); FIG-1, which forms the low-affinity Ca^{2+}-influx system (LACS); and, the vacuolar Ca^{2+} channel, YVC-1. Two of these mutants (Δ*cch-1* and Δ*yvc-1*) exhibited significantly increased tolerance against PAF26 ($p \leq .001$) when compared with the wild type (Figure 1b). The IC_{50} values of Δ*cch-1*

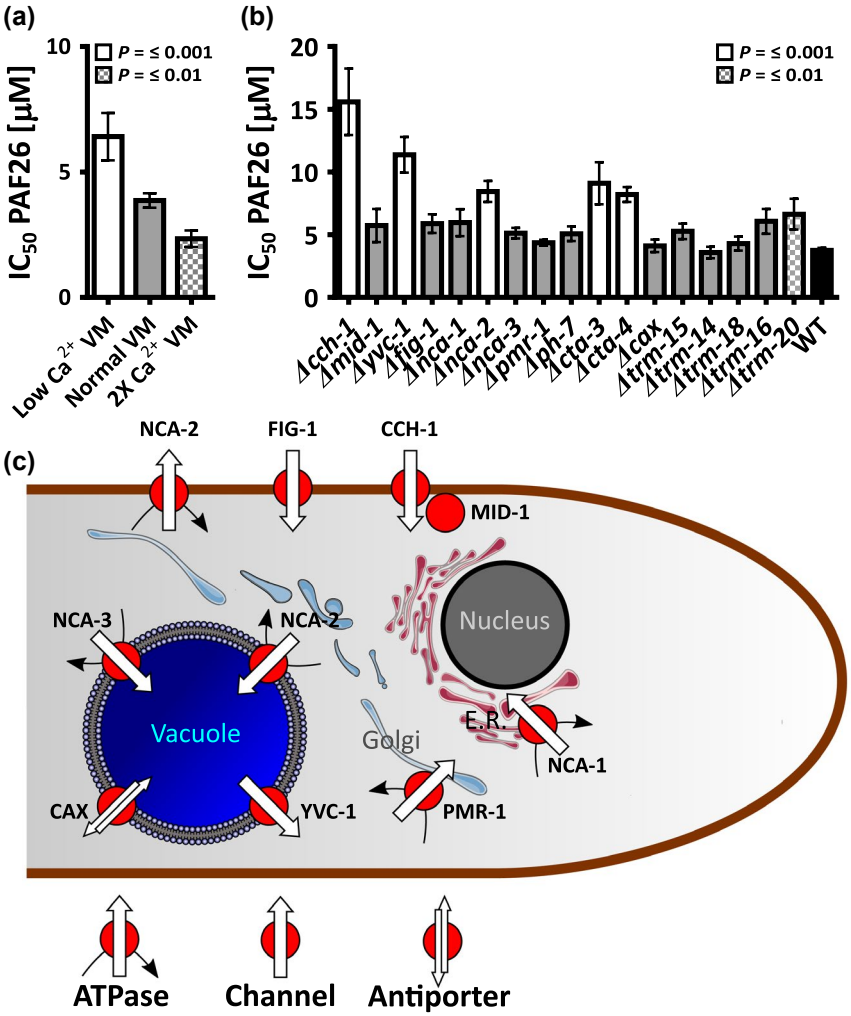

FIGURE 1 Ca^{2+} plays a significant role in the mode-of-action of PAF26. (A) shows the effects of both the removal and increase of free Ca^{2+} in the media on the IC_{50} of PAF26 by fungal cells. Increasing the level lowers the concentration at which PAF26 is effective and removing Ca^{2+} increases the concentration. Both of these results are significant; One-way ANOVA with Dunnet's comparison test: $F(2,12) = 58.85$, $p = \leq .001$, $R^2 = 90.75$, $R^2(\text{adj}) = 89.21$. The Low Ca^{2+} VM ($M = 6.410 \pm 0.941$) was significantly different from the Normal VM ($M = 3.868 \pm 0.288$) at $p = \leq .001$ and the 2X Ca^{2+} ($M = 2.342 \pm 0.331$) was significantly different from Normal VM at $p = \leq .01$ (B) shows the effects of deleting components of the Ca^{2+} homeostasis machinery on susceptibility to PAF26. 6 were significantly more tolerant than the wild type; One-way ANOVA with Dunnet's comparison test: $F(17,106) = 60.13$, $p = \leq .001$, $R^2 = 90.61$, $R^2(\text{adj}) = 89.10$. *Δcch-1* ($M = 15.595 \pm 2.649$), *Δyvc-1* ($M = 11.375 \pm 1.419$), *Δnca-2* ($M = 8.442 \pm 0.838$), *Δcta-3* ($M = 9.099 \pm 1.677$) and *Δcta-4* ($M = 8.212 \pm 0.594$) were significantly more tolerant than the wild type ($M = 3.756 \pm 0.193$) at $p = \leq .001$, and *Δtrm-20* ($M = 6.637 \pm 1.234$) was significant at $p = \leq .01$. Each assay consisted of eight technical and three biological replicates, figures are representative. The predicted localizations of these is shown in (C) based on the localization of their protein orthologs in *S. cerevisiae* yeast cells and vegetative hyphae of *N. crassa* (Wada *et al*., 1987; Yang and Sachs, 1989; Bertl and Slayman, 1990; Diamond *et al*., 1991; Antebi and Fink, 1992; Iida *et al*., 1994; Lapinskas *et al*., 1995; Levina *et al*., 1995; Paidhungat and Garrett, 1997; Erdman *et al*., 1998; Kanzaki, 1999; Benito *et al*., 2000; Locke *et al*., 2000; Muller *et al*., 2001; Palmer *et al*., 2001; Courchesne, 2002; Courchesne and Ozturk, 2002; Denis and Cyert, 2002; Gupta *et al*., 2003; Kaiserer *et al*., 2003; Muller *et al*., 2003; Zhou *et al*., 2003; Zelter *et al*., 2004; Brand *et al*., 2007; Hallen and Trail, 2008; Lew *et al*., 2008; Benito *et al*., 2009; Bormann and Tudzynski, 2009; Bowman *et al*., 2009; 2011; Binder *et al*., 2010; Cavinder *et al*., 2011) [Colour figure can be viewed at wileyonlinelibrary.com]

and Δ*yvc-1* were both above the level (~10 μM) at which PAF26 directly permeabilizes the plasma membrane of *N. crassa* wild-type cells (Muñoz *et al*., 2012).

N. crassa has eight Ca^{2+} ATPases (Zelter *et al*., 2004), for which seven deletion mutants were available as homokaryons for screening: Δ*nca-1*, Δ*nca-2*, Δ*nca-3*, Δ*pmr-1*, Δ*ph-7*, Δ*cta-3*, and Δ*cta-4*. *Δnca-2*, Δ*cta-3*, and Δ*cta-4* exhibited significantly increased tolerance against PAF26 ($p \leq .001$) when compared with the wild type (Figure 1b); with *Δnca-2* approaching inhibitory levels of PAF26 that directly permeabilize the membrane in the wild type.

Homokaryotic deletion mutants of six of the eight predicted *N. crassa* antiporters involved in Ca^{2+} transport (Zelter *et al*., 2004) were available for screening: Δ*cax*, Δ*trm-14*, Δ*trm-15*, Δ*trm-16*, Δ*trm-18*, and Δ*trm-20* (Figure 1b, Table 1). Δ*trm-20* showed significantly greater tolerance ($p \leq .01$) to PAF26 compared with the wild type although this was less than a twofold increase (Figure 1b).

TABLE 1 The half maximal inhibitory concentration (IC_{50}) of PAF26 in Ca^{2+} signaling/homeostasis mutants

	Strain	Genotype	IC_{50} PAF 26 μM	±	Source	*p*
	WT	74-OR23-1V	3.76	0.19	FGSC2489	
Ca^{2+} signaling/ homeostasis	***Δcch-1***	**NCU02762**	**13.94**	**1.26**	**Chu, 2013**	**≤.001**
	Δmid-1	NCU06703	5.74	1.33	FGSC11708	
	Δyvc-1	**NCU07605**	**11.37**	**1.42**	**FGSC11253**	**≤.001**
	Δfig-1	NCU02219	5.89	0.74	FGSC17273	
	Δnca-1	NCU03305	5.96	1.07	FGSC13287	
	Δnca-2	**NCU04736**	**12.73**	**2.37**	**FGSC13071**	**≤.001**
	Δnca-3	NCU05154	5.12	0.42	FGSC13037	
	Δpmr-1	NCU03292	4.36	0.24	FGSC11616	
	Δph-7	NCU08147	5.08	0.59	FGSC11256	
	Δcta-3	NCU07966	9.10	1.68	FGSC11409	≤.001
	Δcta-4	NCU04898	8.22	0.59	FGSC13040	≤.001
	Δena-5	NCU10143	3.27	0.29	FGSC12645	
	Δcax	NCU07075	4.11	0.50	FGSC11249	
	Δtrm-15	NCU00916	5.27	0.62	FGSC11686	
	Δtrm-14	NCU00795	6.19	0.38	FGSC12375	
	Δtrm-18	NCU06366	4.29	0.56	FGSC11408	
	Δtrm-16	NCU02826	6.06	1.00	FGSC11529	
	Δtrm-20	NCU08490	6.64	1.23	FGSC12468	≤.01
	Δplc-1	NCU06245	3.27	0.46	FGSC11411	
	Δplc-2	NCU01266	6.24	1.60	FGSC12022	
	Δplc-3	NCU02175	3.59	0.46	FGSC12023	
	Δplc-4	NCU09655	4.17	0.30	FGSC11271	
	ΔCamK-1	NCU09123	6.99	0.26	FGSC12547	
	ΔCamK-2	NCU02283	5.09	0.36	FGSC12449	
	ΔCamK-3	NCU06177	3.84	0.39	FGSC11536	

Note: Mutants highlighted in bold were tolerant to PAF26 at levels approaching passive membrane permeabilization and were selected for further study.

2.3 | PAF26 is taken up by wild-type macroconidia into vacuoles which fuse and then lyse before releasing the peptide into the cytoplasm

In order to compare the dynamic pattern of peptide-cell interactions between the wild type and the mutants, PAF26 labeled with the fluorophore TAMRA (TMR-PAF26) was imaged. Fluorescent labeling has been previously employed to monitor, using confocal live-cell imaging, the dynamic localization of PAF26 or related peptides in a range of fungi. We are confident that the dynamic pattern of TMR-PAF26 staining provides a faithful localization of the unlabeled peptide in fungal cells and labeled/unlabeled peptides have similar IC_{50} values (Muñoz *et al*., 2012; 2013a; 2013b). Previously it has been shown that wild-type macroconidia treated with a low fungicidal concentration of FITC-PAF26 (2.5 μM) exhibit a similar time-dependent staining pattern as germlings treated with the same concentration of PAF26 (Muñoz *et al*., 2012). A similar localization pattern of TMR-PAF26 interaction, internalization and distribution was observed with ungerminated macroconidia to that of FITC-PAF26. The use of macroconidia allowed a basic monitoring of cell volume, surface area and developmental state in relation to possible variations in morphogenesis and staining patterns.

2.4 | The dynamic pattern of TMR-PAF26 in Ca^{2+} homeostasis mutant staining provides insights into the localization and roles of the defective mutant proteins

In order to gain more insight into which stages of the PAF26 interaction, uptake and distribution process the CCH-1, YVC-1, and NCA-2 proteins influence, the time-dependent staining by TMR-PAF26 in each of the *Δcch-1*, Δ*yvc-1*, and *Δnca-2* mutants were compared with that in the wild type. As a baseline for the comparison, four staining patterns were identified in the wild-type macroconidia that could be readily quantified at 30 min intervals following treatment with 3.5 μM TMR-PAF26. These staining patterns related to different events in the time-dependent uptake and distribution to different organelles which precedes eventual cell death, initially determined by YO-PRO-1/Propidium Iodide staining. They were: (a) Accumulation in multiple small vesicles. These were predicted to be mostly endosomes typically up to ~1 μm in width. (b) Accumulation in 1–3 large vacuole(s) typically greater than ~1.5 μm in width. (c) Accumulation in the cytoplasm and excluded from vacuoles. This is the stage just after the peptide has been released out from vacuoles. (d) Accumulation in both the cytoplasm and vacuoles. This is the stage after which the intracellular membranes have become permeabilized and thus represents commitment to cell death, as previously reported (Muñoz *et al*., 2012).

In the wild-type macroconidia (Figures 2b and 3a), this quantitative analysis showed that after treatment for 30 min with TMR-PAF26, all the macroconidia had interacted with TMR-PAF26 and many were beginning to internalize the peptide into small vesicles. After 60 min, many of the conidia had already undergone vacuolar expansion and some had exported the peptide into the cytoplasm, and this correlated with a transient reduction in the percentage of cells with peptide only localized within small vesicles. After 60 min, 40% of the cells had actively transported the peptide out of their vacuoles and into the surrounding cytoplasm. In another 40% of the cells at the 60 min time point, vacuolar membrane permeabilization had occurred and the peptide had equilibrated throughout the cells. By 120 min, 57% of the cells were permeabilized (Figures 2b and 3a).

2.5 | YVC-1 is required for transport of PAF26 from vesicles to vacuoles

When the Δ*yvc-1* mutant was treated with the labeled peptide (Figures 2b and 3b), it rapidly appeared at the cell envelope. Unlike with the wild type, the peptide was internalized into small vesicles at a more-or-less linear rate with much remaining trapped at the cell surface. Accumulation of the peptide in vacuoles was much slower and reached a maximum of 6% of the cells with this localization pattern after 120 min. Virtually no cells were observed with peptide exclusively in the cytoplasm at the three time points of measurement over the 120 min by which time only 5% of cells were internally permeabilized. After 120 min, 79% of the Δ*yvc-1* cells had taken up TMR-PAF26 compared with 100% in the wild type. Thus, less TMR-PAF26 was taken up by Δ*yvc-1* cells, most accumulated in small vesicles and few cells had internal membrane permeabilization after 120 min (5% compared with 57% in the wild type). These results are consistent with YVC-1 being required for the transport of PAF26 from vesicles to vacuoles.

2.6 | NCA-2 is required for the interaction of PAF26 and the cell envelope

When the Δ*nca-2* mutant was treated with TMR-PAF26 (Figures 2b and 3c) the cell envelopes of the macroconidia were visibly less fluorescent than that of the wild type. Thus, the affinity of TMR-PAF26 for the cell envelope of this mutant seemed to be reduced and its staining was delayed compared with that of the wild type. The Δ*nca-2* macroconidia also internalized TMR-PAF26 at a far reduced rate compared with the other mutants and the peptide mostly became trapped within the small vesicles, resulting in virtually no TMR-PAF26 being taken up by vacuoles and a correspondingly extremely small percentage (~2%) of the cells having permeabilized internal membranes after 120 min (Figure 2b).

2.7 | CCH-1 plays a key role in the energy- and Ca^{2+}-dependent internalization of PAF26 by fungal cells

The pattern of TMR-PAF26 internalization and intracellular transport within macroconidia of the *Δcch-1* mutant appeared to be

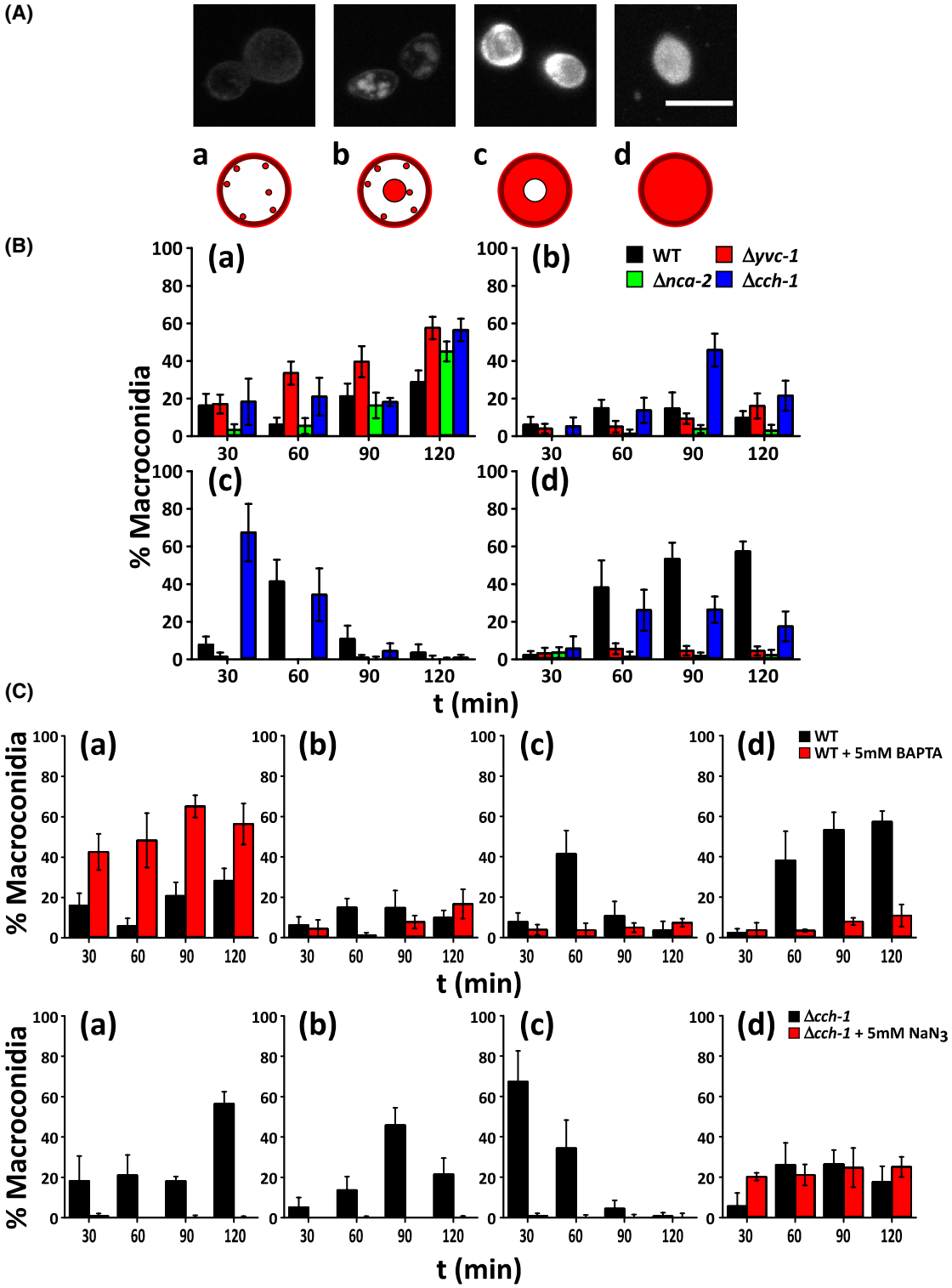

FIGURE 2 Graphical representation showing that the interaction between PAF26 and macroconidia is altered through deletion of Ca^{2+}-channels and pumps. (A) shows maximum intensity projections from a Z series captured using confocal microscopy. Initially, the peptide appears at the cell envelope and within small vesicles (a). The peptide is then accumulated in larger vesicles and vacuoles (b) until there appears a lower number of larger vacuoles (c) which will eventually fuse into a single vacuole which then releases the peptide into the cytoplasm (d). Scale bar is 5 μm. (B) shows quantification of this interaction over time for the deletion mutants compared to the wild type; there are marked changes in the localization of the peptide during the time course. (C) shows the interaction between PAF26 and macroconidia is Ca^{2+}-dependent and energy dependent. This is demonstrated by the significant delay in the uptake of PAF26 in the wild type when extracellular free Ca^{2+} is removed using BAPTA, at top. The peptide remains trapped in small vesicles and there is little transport into the vacuolar system and consequently a reduction in internal membrane permeabilization. The lower figure shows the effect of the removal of cellular free energy on the *Δcch-1* mutant using the metabolic inhibitor NaN_3. There is no uptake of PAF26 into the cell and, therefore, the direct translocation across the plasma membrane must be an energy-dependent process. *N* = 100 macroconidia minimum per field of view, 10 fields of view per time point, repeated at least twice [Colour figure can be viewed at wileyonlinelibrary.com]

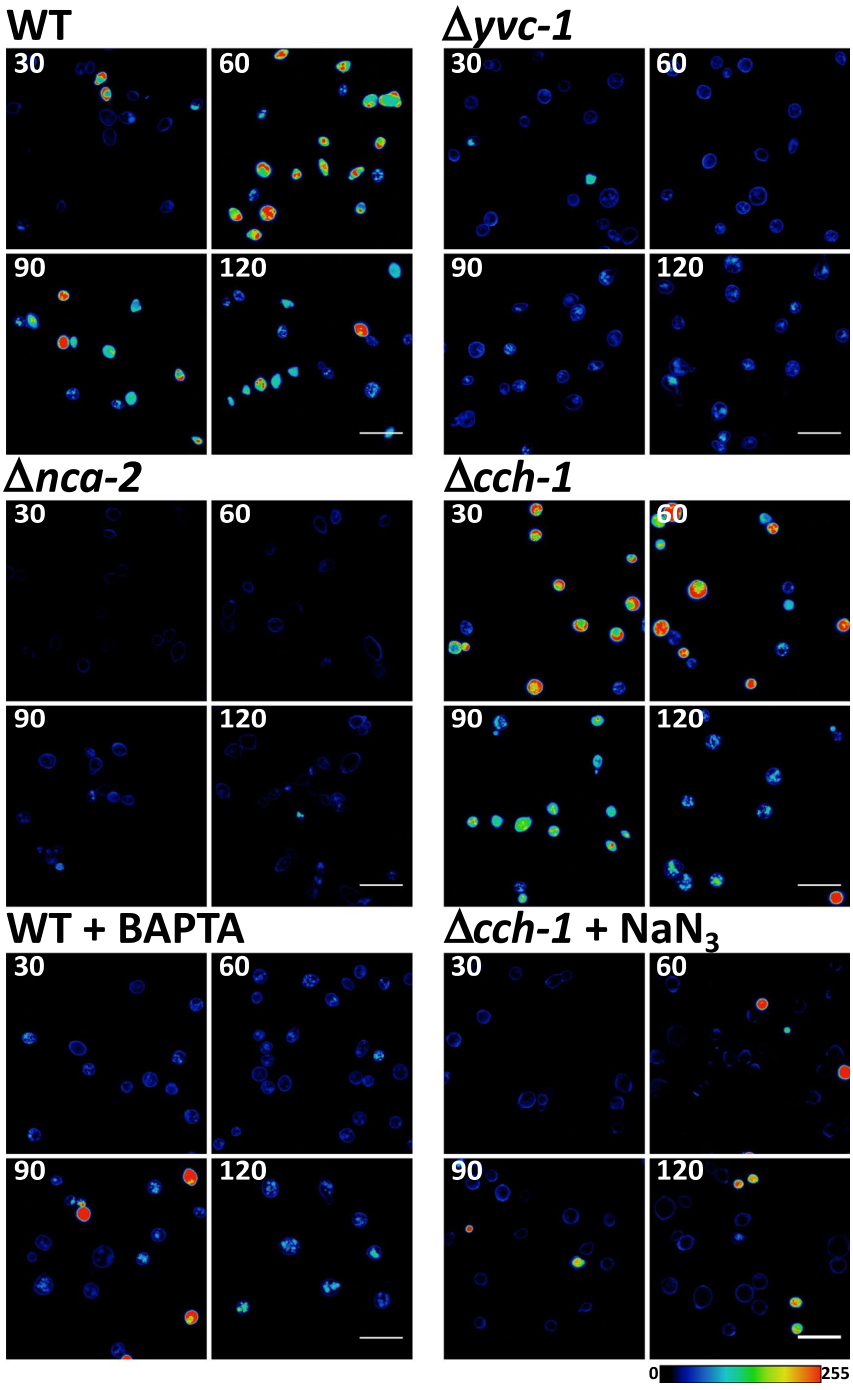

FIGURE 3 The interaction with PAF26 is altered through deletion of Ca^{2+}-channels and -pumps as shown by visualization of wild-type and mutant conidia stained with 3.5 μM TAMRA labeled PAF26. These figures show maximum intensity projections of Z stacks false colored with the "physics" lookup table to highlight the different fluorescent intensities measured. (A) The wild-type conidia undergo a sequence of events which ultimately results in cell death (Muñoz *et al.*, 2012). (B) The *Δyvc-1* mutant retains the peptide in small vesicles, without the formation of a large central vacuole, as in the wild type. (C) The *Δnca-2* mutant appears much reduced in peptide interaction, with very few conidia showing the peptide bound to the envelope. (D) The process is reversed in the *Δcch-1* mutant, where the peptide first appears within the cytoplasm and is pumped into small vesicles which then appear to fragment. No conidia were seen to completely lose loaded peptide. The internalization process is Ca^{2+} dependent and energy-dependent, as chelation of Ca^{2+} with BAPTA (E), and treatment with Sodium azide (NaN_3) (F), significantly reduced uptake of TAMRA-PAF26. 1,000 individual macroconidia per time point per strain. Assay was repeated twice and images are representative. Scale bar is 20 μm [Colour figure can be viewed at wileyonlinelibrary.com]

opposite to that in the wild type (Figure 3d). After treatment for 30 min the peptide was primarily localized in the cytoplasm (in 67% of cells) and to a much lesser extent in small vesicles (~18% of cells) and to a very low level in large vacuoles (~5% of cells). Between 30 and 90 min, TMR-PAF26 was removed from the cytoplasm and increased in amount in the small vesicles and large vacuoles. Between 90 and 120 min the large vacuoles containing TMR-PAF26 are fragmenting into smaller vesicles. This was reflected by a dramatic increase in the number of stained small vesicles (Figure 2b).

The overall rate of internalization of TMR-PAF26 by *Δcch-1* macroconidia was faster than in the wild type because in the former it was initially taken up directly into the cytoplasm while in the latter it first appeared intracellularly in small vesicles that are presumed to be mostly endosomes. It seems unlikely that TMR-PAF26 is taken up by means of non-specific permeabilization of the plasma membrane because this would likely have resulted in rapid cell death. Furthermore, 30 min after the addition of TMR-PAF26 it was clear that the vacuolar membrane had not become permeabilized because the peptide was excluded from the vacuoles of cells in which the cytoplasm was fluorescent.

In order to clarify whether the passage of PAF26 across the plasma membrane into the cytoplasm of the *Δcch-1* mutant was a result of passive translocation or active uptake, macroconidia were pre-treated with the metabolic inhibitor NaN_3 (Muñoz *et al.*, 2012)

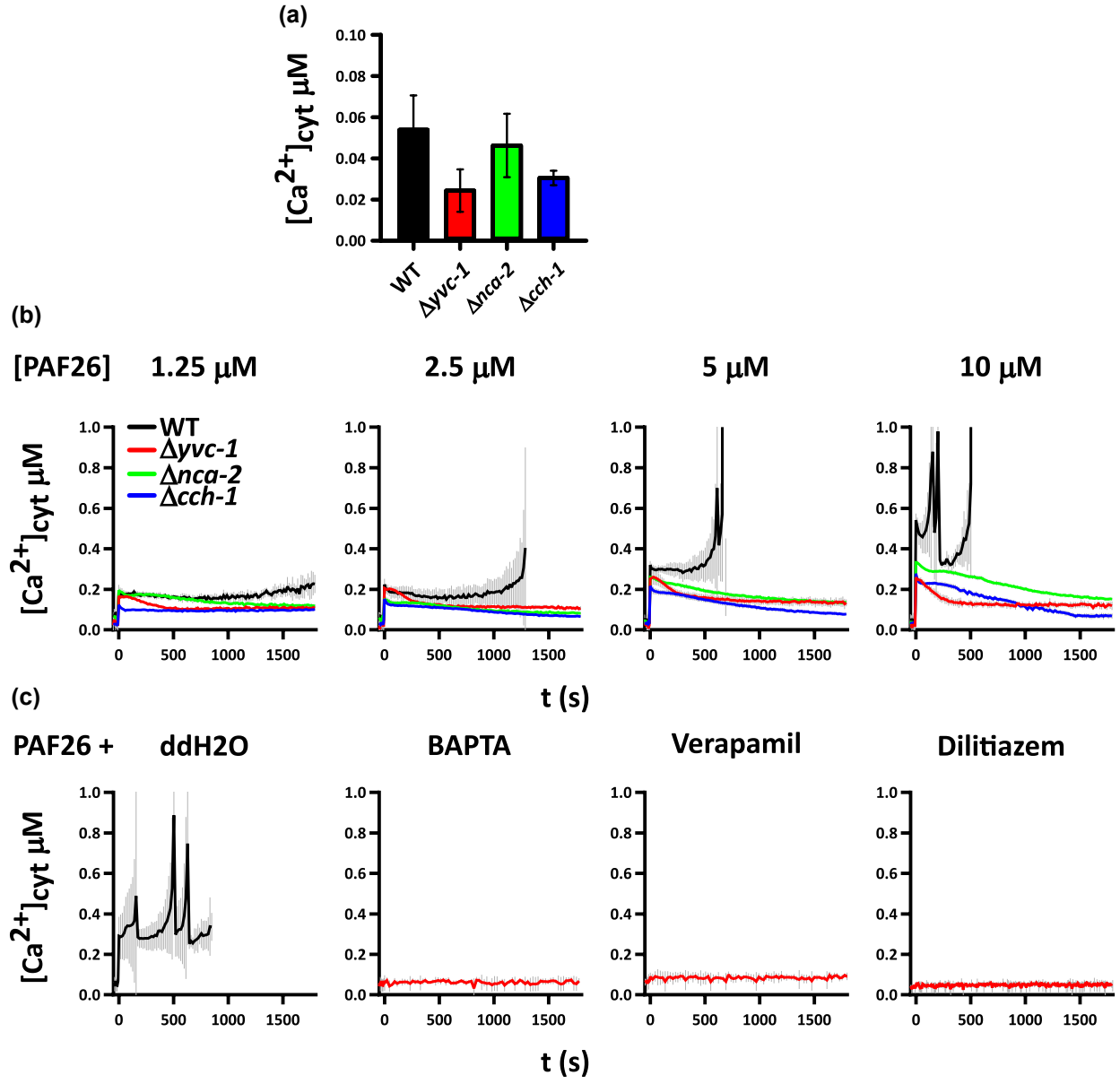

FIGURE 4 The $[Ca^{2+}]_{cyt}$ response to PAF26 is altered by deletion of Ca^{2+} channels and pumps. (A) shows the unstimulated resting level of the wild type and the Ca^{2+} homeostatic mutants: the resting level in *Δyvc-1* and *Δcch-1* were significantly different from the wild type. One-way ANOVA with Dunnet's comparison test: $F(3,108) = 32.83$, $p = \leq.001$, $R^2 = 47.70$, $R^2(\text{adj}) = 46.24$. (B) shows the $[Ca^{2+}]_{cyt}$ response to PAF26 by population wide measurements using the genetically encoded reporter aequorin supplied with an excess of coelenterazine. The [PAF26] µM is shown above each measurement series and was added at time 0, baseline measurements were recorded for 50s before the addition of the peptide. (C) shows that this response in the wild type is both dependent on external Ca^{2+} and on the presence of an external Ca^{2+} channel, the biphasic response to 5µM PAF26 (seen in the ddH_2O control) is completely abolished following chelation of Ca^{2+} with BAPTA or treatment with L-Type Ca^{2+} channel blockers. All measurements are averages of six individual wells in a 96-well plate, with $[Ca^{2+}]_{cyt}$ calculated following quenching of the remaining aequorin using EtOH and Ca^{2+}. Error bars are standard deviations. All experiments were repeated a minimum of three times and the above figures are representative [Colour figure can be viewed at wileyonlinelibrary.com]

at a concentration of 5 µM for 15 min before the addition of TMR-PAF26 and subsequent imaging and quantification of localization over 120 min (Figures 2c and 3f).

In the presence of NaN_3, over the whole 120 min period of incubation with TMR-PAF26, the peptide remained bound to the cell envelope and was not internalized by most of the macroconidia. Clearly the metabolic inhibitor NaN_3 had almost completely abolished the movement of TMR-PAF26 across the plasma membrane indicating that the uptake of the peptide into the cells of the *Δcch-1* mutant is an ATP-dependent process. The results also showed that the rate of internal membrane permeabilization, while faster over the first 30 min, remained similar to that of the non-azide treated *Δcch-1* cells; after 120 min ~ 25% of the cells were fluorescent throughout the cell. These results are consistent with the uptake of TMR-PAF26 by this subpopulation of *Δcch-1* macroconidia being energy independent as a result of a passive process.

These results are consistent with the normal endocytic internalization of PAF26 being dependent on the Ca^{2+} channel protein, CCH-1. As CCH-1 appears to initiate PAF26 internalization by endocytosis (see previous section), this suggests that the uptake of Ca^{2+} from the external medium may be mediated by this Ca^{2+} channel, which has previously been reported to be immunolocalized to the plasma membrane (Locke *et al*., 2000). Furthermore, we had previously shown that removal of Ca^{2+} from VM made macroconidia more resistant to being killed by PAF26. To attempt to mimic the effect of *cch-1* deletion in the wild type, Ca^{2+} was removed from the external medium by the addition of the Ca^{2+} chelator BAPTA (5 mM) 30 min prior to the TMR-PAF26 treatment (Figures 2c and 3e). Rather than preventing the entry of the peptide, the BAPTA treatment had the unexpected effect of trapping the peptide in small vesicles. Over the 120 min period very little TMR-PAF26 had localized in large vacuoles, in the cytoplasm and only ~11% of the macroconidia had fluorescence throughout the cell. The phenotype of the *Δcch-1* mutant is consistent with the CCH-1 protein playing a key role in the energy- and Ca^{2+}-dependent internalization of PAF26 by fungal cells.

2.8 | The $[Ca^{2+}]_{cyt}$ response during PAF26 treatment is disrupted in the $[Ca^{2+}]_{ext}$ tolerant mutants

The wild type had previously been shown to undergo a dose dependent biphasic rise in $[Ca^{2+}]_{cyt}$ upon addition of PAF26 at concentrations between 0.8 and 2.0 μM (Muñoz *et al*., 2012). The experiment was repeated here but with over a concentration range of 1.25-10 μM PAF26. For all measurements, the unstimulated $[Ca^{2+}]_{cyt}$ resting level was measured for 50 s, in the wild type this was calculated to be 0.05 ± 0.02 μM (Figure 4a), before the peptide was added at time 0. After treatment with a low final concentration of PAF26 (1.25 μM), an immediate increase in $[Ca^{2+}]_{cyt}$ to 0.19 ± 0.01 μM was observed and this was sustained throughout the measurement period (1,200 s) and slightly increased toward the end of this period (Figure 4b). When the PAF26 added was at a final concentration of 2.5 μM, which is close to its IC_{50} value, the initial increase in $[Ca^{2+}]_{cyt}$ was slightly greater (to 0.22 ± 0.03 μM) (Figure 4b). Again, this was followed by a period of sustained $[Ca^{2+}]_{cyt}$ increase, but there was also a more pronounced exponential increase in $[Ca^{2+}]_{cyt}$ which began at ~900 s after treatment. With the higher dose, there was also an increase in the standard deviations of the measurements with time. This is due to aequorin consumption during the course of the experiment, resulting in less sensitivity after prolonged exposure to high $[Ca^{2+}]$ (note that luminescence measurements from six wells are averaged per time point). When the wild type was treated with 5 μM PAF26, which was above its IC_{50} value, the $[Ca^{2+}]_{cyt}$ response followed the same general pattern but with a much larger initial $[Ca^{2+}]_{cyt}$ increase to 0.32 ± 0.02 μM and a shorter period of sustained increase before the $[Ca^{2+}]_{cyt}$ increase became exponential at ~430 s (Figure 4b). Furthermore, after 590 s following peptide treatment, $[Ca^{2+}]_{cyt}$ spiking was observed. The $[Ca^{2+}]_{cyt}$ response was further accentuated after treatment with a very high dose (10 μM) of PAF26 resulting in a rapid initial rise in $[Ca^{2+}]_{cyt}$ to 0.54 ± 0.03 μM, followed by an immediate exponential increase in $[Ca^{2+}]_{cyt}$. This in turn was followed by the $[Ca^{2+}]_{cyt}$ spiking and then a sudden drop in $[Ca^{2+}]_{cyt}$ after ~220 s, which then exponentially increased and subsequently underwent spiking again (Figure 4b).

The unstimulated resting level of $[Ca^{2+}]_{cyt}$ in the Δ*yvc-1* mutant was measured as 0.02 ± 0.01 μM (Figure 4a), significantly different at $p > .01$. The $[Ca^{2+}]_{cyt}$ response of the Δ*yvc-1* strain to PAF26 was markedly different to that of the wild type. While there was a similar initial immediate, dose dependent increase in $[Ca^{2+}]_{cyt}$, there was no second exponential increase in $[Ca^{2+}]_{cyt}$, which was particularly evident after treating the wild type with PAF26 at 2.5 μM or above (Figure 4b). Instead the Δ*yvc-1* mutant underwent a slight reduction in $[Ca^{2+}]_{cyt}$ followed by a sustained, more-or-less constant $[Ca^{2+}]_{cyt}$ level that was significantly raised compared with the unstimulated resting levels recorded prior to treatment. Thus the Δ*yvc-1* mutant lacked the second $[Ca^{2+}]_{cyt}$ increase of the biphasic $[Ca^{2+}]_{cyt}$ response of the wild type, which is consistent with this second $[Ca^{2+}]_{cyt}$ increase resulting from the release of Ca^{2+} from the vacuole. The resting level of $[Ca^{2+}]_{cyt}$ in the Δ*nca-2* mutant was measured at 0.05 μM ± 0.02, Figure 4a, and was not significantly different from the wild type. In general terms, the Δ*nca-2* mutant showed a similar response to PAF26 as did the Δ*yvc-1* mutant. However, the Ca^{2+} signatures of the Δ*nca-2* and Δ*yvc-1* mutants were clearly but not dramatically different from each other; there was a more pronounced dose dependent $[Ca^{2+}]_{cyt}$ increase in the Δnca-2 strain compared with that in Δ*yvc-1* in response to PAF26 (Figure 4b). The resting level of $[Ca^{2+}]_{cyt}$ in the Δ*cch-1* mutant was 0.03 ± 0.00 μM Figure 4a, significantly different to the wild type at $p > .01$. Interestingly, deletion of *cch-1* does not inhibit the initial increase in $[Ca^{2+}]_{cyt}$ after PAF26 addition, surprising given the lack of evidence for another Ca^{2+} channel at the cell surface. The Ca^{2+} signatures of the Δ*cch-1* mutant in response to different concentrations of PAF26 were broadly similar to those of the Δ*yvc-1* and Δ*nca-2* mutants (Figure 4b). Thus the Δ*cch-1* mutant also showed an initial $[Ca^{2+}]_{cyt}$ increase but lacked the second $[Ca^{2+}]_{cyt}$ increase of the typical biphasic response of the wild type to PAF26. These results suggest there may be an unidentified L-type channel within the plasma membrane, not CCH-1, being responsible for the initial $[Ca^{2+}]_{cyt}$ increase in response to PAF26.

The influence on the $[Ca^{2+}]_{cyt}$ response to 5.0 μM PAF26 of the wild type following pre-treatment with 5 mM BAPTA (to chelate extracellular Ca^{2+}) or with the L-type Ca^{2+} channel blockers diltiazem or verapamil (both at 5 mM), was analyzed (Figure 4c). A 15 min pre-treatment with ddH_2O (the control) caused a biphasic increase in $[Ca^{2+}]_{cyt}$ while all of the other treatments prevented any significant $[Ca^{2+}]_{cyt}$ increase (Figure 2). These results are consistent with the biphasic $[Ca^{2+}]_{cyt}$ increase being dependent on extracellular Ca^{2+} as reported before (Muñoz *et al*., 2012) and on L-type Ca^{2+} channel activity. The only known L-type Ca^{2+} channel in *N. crassa* is CCH-1(Zelter *et al*., 2004). These results also suggest that the second component of the biphasic $[Ca^{2+}]_{cyt}$ increase is dependent on the first $[Ca^{2+}]_{cyt}$ increase.

2.9 | Imaging using the fluorescent reporter GCaMP6 shows PAF26 does not cause a dose dependent rise in $[Ca^{2+}]_{cyt}$

In order to investigate whether PAF26 was indeed causing a dose dependent rise in $[Ca^{2+}]_{cyt}$, conidia expressing GCaMP6s were imaged during PAF26 treatment using widefield fluorescence microscopy. Individual macroconidia were then isolated from the background in FIJI and fluorescence measured over time. As Figure 5a shows, the individual responses are far more varied than the measurements using aequorin suggested. In the middle of the time course, the moment the PAF26 reaches the field of view and interacts with the cells can be clearly seen in a sudden increase in Ca^{2+} spiking in all the individuals. Given that the aequorin measurements are across a whole population, it is not hard to see how the cumulative effects of an increase in Ca^{2+} spikes and waves could be interpreted as a dose dependent rise in $[Ca^{2+}]_{cyt}$.In order to determine whether there was a predictable response to PAF26 addition, several repeated experiments were run in which the peptide was added and fluorescence intensity recorded. No distinct pattern or regularity was found within any of the data sets, except for an increase in Ca^{2+} signaling after PAF26 addition. As the only noticeable response, the amplitude and frequency of these

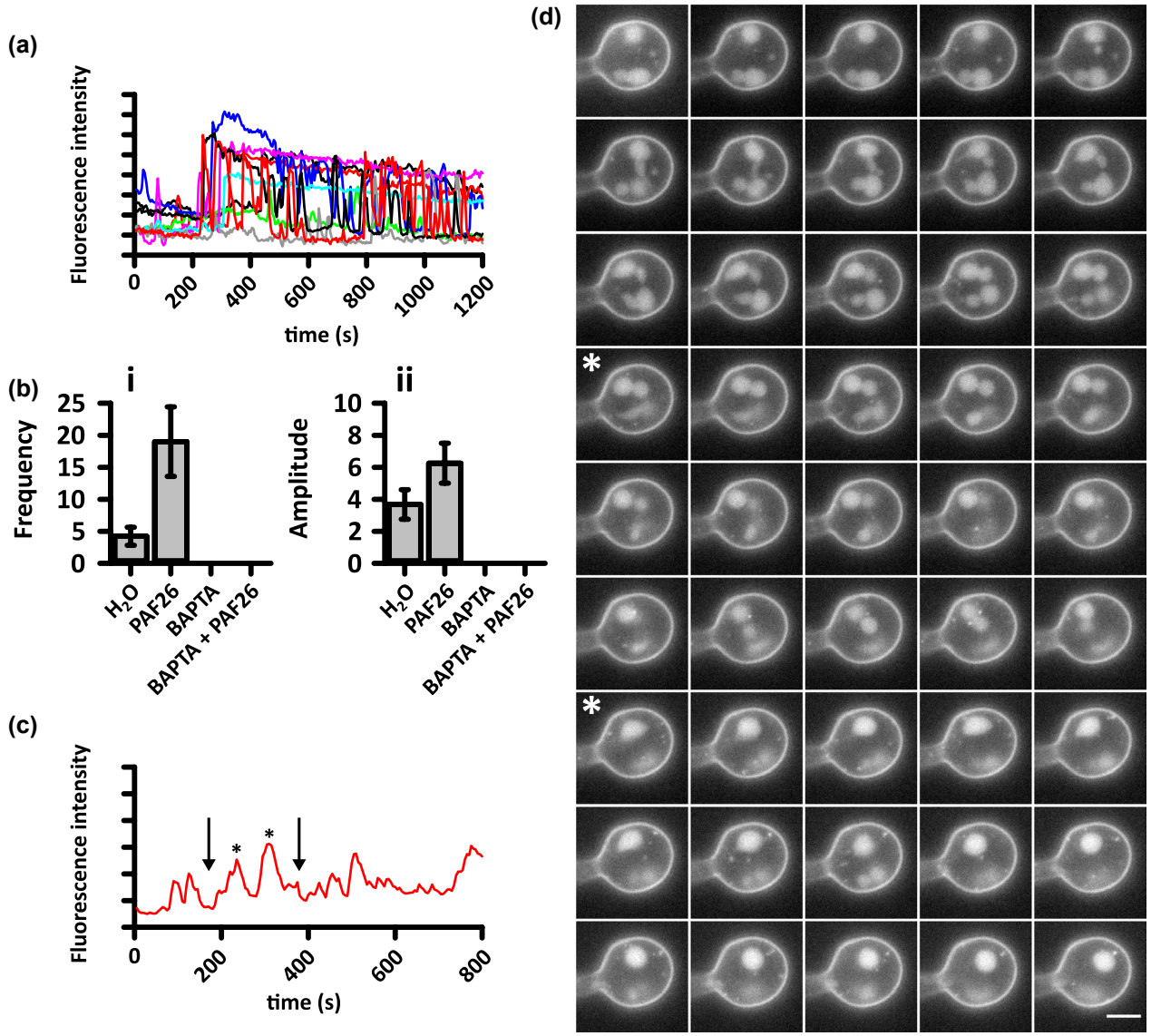

FIGURE 5 PAF26 does not cause a dose-dependent rise in $[Ca^{2+}]_{cyt}$. (A) shows the relative fluorescence intensity of several macroconidia expressing GCaMP6s during PAF26 treatment. Fluorescence values are normalized and given as arbitrary values. After the addition of PAF26 there is a marked increase in the amplitude and frequency of Ca^{2+} spiking. (B) Quantification of this revealed an actual increase in spiking from an average of four spikes per 30 min to 19 spikes per 30 min (i). The spiking was entirely dependent on the presence of external Ca^{2+} as chelation with BAPTA reduced the frequency of spiking to 0. The amplitude of the individual spikes also increased from 4 to 6 arbitrary units (ii). (C) these spikes often appeared to correspond to the meeting of vesicles and vacuoles within the cell; the images captured between the two arrows are shown in (D) which shows wide field fluorescence images captured every 5 s. The two spikes marked by * in C appear to correspond to vacuolar fusion events. Scale bar = 2μm [Colour figure can be viewed at wileyonlinelibrary.com]

Ca^{2+} spikes was quantified. Conidia were treated either with ddH_2O or ddH_2O containing 3.5 μM PAF26. A second set were pre-treated with 5 mM BAPTA before ddH_2O or PAF26 treatment. The conidia treated with ddH_2O have a relatively low frequency of Ca^{2+} spiking with the mean being 4 spikes over the course of the measurement. This is consistent with our findings as to the rate of Ca^{2+} spiking in germinating and fusing conidia (Read, unpublished). When the cells are treated with PAF26 however, there is a marked increase in both frequency and amplitude. The mean frequency of the Ca^{2+} spikes increases to 19 and the amplitude increases to around 6 times the resting level from 4 (Figure 5b). Both of these results are significant at $p < .01$. When the conidia are pre-treated with BAPTA however, all Ca^{2+} spiking ceases completely. While there were no apparent recurring patterns in the spiking events, observations appeared to show that they correspond to vesicles and vacuoles coming into close proximity. A Ca^{2+} trace is shown in Figure 5c and images are shown in Figure 5d. The images shown in Figure 5d are taken every five seconds from the timeframes indicated by the black arrows in Figure 5c. The first Ca^{2+} spike marked by *, appears to correspond with the meeting of the two vacuoles at the lower part of the image, whether they fuse or not is unclear. In the images corresponding to the second spike marked with *, the fusion of two vacuoles is clear at the top of the image.

3 | DISCUSSION

3.1 | Ca^{2+} plays important roles in the mode-of-action of PAF26

In this research, evidence for Ca^{2+} signaling and homeostasis having a significant role in the PAF26 mode-of-action was obtained initially by testing the PAF26 sensitivity of conidia grown in the presence or absence of calcium. When the level of calcium in the media is kept at a minimal level, tolerance increases. Conversely when the level is raised, tolerance decreases. This was confirmed with deletion mutants defective in different components of their cellular transport machinery of Ca^{2+}. Deletion of most of the Ca^{2+} channels significantly increased the concentrations at which PAF26 inhibits fungal growth. The elimination of the high affinity Ca^{2+} plasma membrane channel CCH-1 and the vacuolar channel YVC-1 as well as the Ca^{2+} ATPase resulted in inhibitory concentrations of the peptide approaching the point at which passive membrane permeabilization occurs. Ca^{2+} has been shown to be an important factor in the mechanistics of PMAP-23 against *Candida albicans*, the disruption results in reactive oxygen species (ROS) accumulation which triggers apoptosis (Kim and Lee, 2019). This effect is also seen in the peptide CGA-N9 against *C. tropicalis* (Li *et al*., 2019). High levels of cytosolic free Ca^{2+} have also been shown to confer protection to *C. albicans* against the antimicrobial MUC7 12mer, thought to be by a resulting change in the cell membrane properties preventing peptide entry (Lis *et al*., 2010). It appears in this case that the elevated levels of cytosolic free Ca^{2+} are a stress response designed to maximize survival by initiating the endocytosis of PAF26. There are significant changes to the pattern of peptide cell interaction in the mutants and to the quantity of peptide the mutants take up. The mutations in the Ca^{2+} distribution machinery appear to disrupt the internalization and accumulation of the peptide which in turn increases tolerance to PAF26. Deletion of *nca-2* appears to influence the binding of PAF26 to the cell envelope, the *Δnca-2* mutant has been shown to accumulate up to 10 fold more Ca^{2+} than wild-type cells, suggesting that NCA-2 serves to remove Ca^{2+} from the cell (Bowman *et al*., 2011). We found no significant difference in the resting level of $[Ca^{2+}]_{cyt}$ from the wild type however under unstimulated conditions. Interestingly however, the *Δnca-2* mutant has a membrane potential reversed from the wild type due to a lack of cell surface H^+ATPase function (Hamam and Lew, 2012). In *S. cerevisiae* the H^+ATPase is one of the most abundant cell surface proteins (Bagnat *et al*., 2001) and makes up a significant amount (up to 10%) of the cell surface in *N. crassa* (Bowman *et al*., 1981). PAF26 has been shown to cause a rapid depolarization of the membrane in wild-type cells in an energy-independent manner (Muñoz *et al*., 2012). Given that PAF26 has a net positive charge, the membrane potential reversed *Δnca-2* should technically not be inhibited in PAF26 membrane binding from an electrostatic view. It is, therefore, possible to propose that PAF26 directly inhibits H^+-ATPase action, possibly by direct binding; misfunctioning H^+--ATPase at the plasma membrane is sent to the vacuole for degradation in yeast, a possible mechanistic for the accumulation of PAF26 (Bagnat *et al*., 2001; Liu *et al*., 2006). When the peptide is internalized in the *Δyvc-1* mutant, it remains in small vesicles with very little sign of the peptide entering the vacuolar system; adding support for the hypothesis that YVC-1 and a threshold amount of PAF26 is required to initiate vacuolar fusion. Vacuolar fusion occurs through conformational change of the docking SNARE proteins, triggered by the release of Ca^{2+} from the vacuole in *S. cerevisiae* (Bayer *et al*., 2003; Merz and Wickner, 2004; Coonrod *et al*., 2013). In *S. cerevisiae*, isolated vacuoles are able to catalyze their own fusion through the release of Ca^{2+} from yvc1p present in the vacuolar membrane (Peters and Mayer, 1998). This does not appear to be the case in *N. crassa* however, as both deletion of YVC-1 and removal of extracellular Ca^{2+} resulted in the trapping of the peptide in small vesicles. Therefore, extracellular Ca^{2+} is required to initiate the release of Ca^{2+} from the vacuoles and trigger fusion. This raises questions as to why internal membrane fusion is reliant on external stimuli. In the *Δcch-1* mutant the peptide was directly translocated across the plasma membrane into the cytoplasm in an energy dependent manner, before accumulation in vacuoles, meaning PAF26 does not kill by being present in the cytosolic space. CCH-1 is, therefore, required to initiate the endocytic pathway. Energy dependent peptide uptake into the vacuolar system is also seen in the *Penicillium chrysogenum Penicillium* antifungal protein B (PAFB), where the fungal cells show no signs of cell death as long as the peptide remains in the vacuole (Huber *et al*., 2018). This is similarly seen in the *Neosartorya (Aspergillus) fischeri* antifungal protein (NFAP), which is also accumulated in the vacuole in an energy dependent maner.

Again, this peptide also does not exert its antifungal effects until it is present within the cytoplasm (Hajdu *et al*., 2019). This contrasts the findings here of PAF26 being present within the cytoplasmic space without killing the cells. The importance of the vacuole in the mode of action of many AFPs is becoming increasingly apparent. A genetic screen of *S. cerevisiae* revealed tolerance to the plant antifungal defensins NbD6 and SBI6 could be increased by deletion of genes involved in vacuolar transport (Parisi *et al*., 2019).

Ca^{2+} measurement at the population level revealed that the Ca^{2+} responses to PAF26 were markedly different in the PAF26 tolerant mutants. While all underwent a similar initial increase in $[Ca^{2+}]_{cyt}$ the second biphasic increase seen in the wild type was abolished. This initial increase was independent of CCH-1, as the signal in the Δ*cch-1* mutant increased, but was dependent on external Ca^{2+} and L-type Ca^{2+} channels. The fact that L-type channel blockers completely stop the $[Ca^{2+}]_{cyt}$ increase as does the chelation of external Ca^{2+} using BAPTA would suggest that there is another, as yet unknown cell surface Ca^{2+} channel. These findings mirror those of Binder *et al*. (2010), who found that deletion of *cch-1* did not prevent the increase in $[Ca^{2+}]_{cyt}$ in response to *P. chrysogenum Penicillium* antifungal protein (PAF). When these measurements were taken at the level of the individual, rather than the population, it became apparent that PAF26 does not in fact cause a dose dependent rise in $[Ca^{2+}]_{cyt}$ but rather increases both the amplitude and frequency of Ca^{2+} spiking, again dependent on the presence of external Ca^{2+}. These findings have allowed us to propose the model shown in Figure 6 for the role of Ca^{2+} signaling and homeostasis in the mode of action of PAF26. Now the challenge is to identify the trigger of vacuolar release of PAF26 and the initiator of cell death.

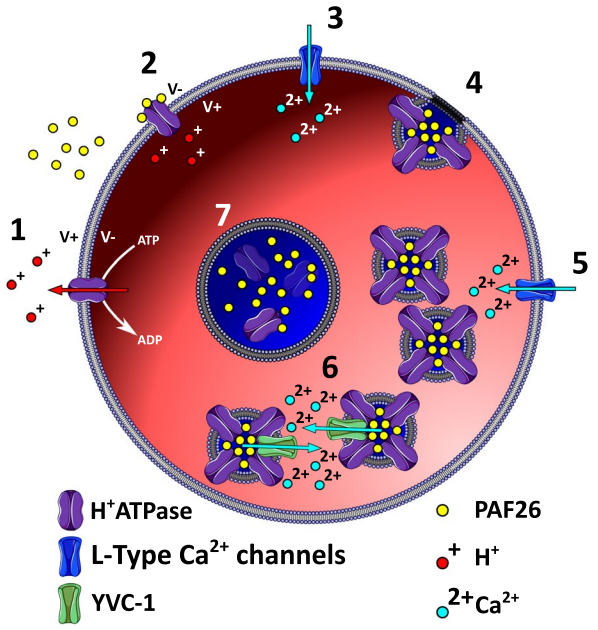

FIGURE 6 Proposed role of Ca^{2+} signaling in the mode of action of PAF26. (1) initially the cell is unstimulated and maintains a low $[Ca^{2+}]_{cyt}$ and stable membrane potential. (2) PAF26 inhibits the cell surface H^+ATPase initiating membrane depolarization. (3) Depolarization of the plasma membrane activates the voltage gated CCH-1, causing $[Ca^{2+}]_{cyt}$ to rise. (4) This rise in $[Ca^{2+}]_{cyt}$ initiates the turnover of the H^+ATPase including bound PAF26 by endocytosis. (5) further rises in $[Ca^{2+}]_{cyt}$ caused by external Ca^{2+} entering through CCH-1 initiate Ca^{2+} release through YVC-1 (6) driving the fusion of membranes. (7) PAF26 is released from the H^+ATPase as it is degraded and accumulates in the vacuolar system [Colour figure can be viewed at wileyonlinelibrary.com]

4 | MATERIALS AND METHODS

4.1 | *Neurospora crassa* stocks

N. crassa strains were obtained from the Fungal Genetics Stock Centre (FGSC, University of Missouri, Kansas City, USA), unless otherwise specified. FGSC2489 (*matA*,74-OR23-1VA) was used as the wild-type control. *N. crassa* strains generated in this study were derived from FGSC9717 (*matA*,*Δmus-51::bar*$^+$; *his-3*$^-$), FGSC9720 (*matA*,*Δmus-52::bar*$^+$; *his-3*$^-$) and FGSC6103 (*matA*,*his-3*$^-$) *N. crassa* was cultured and maintained according to FGSC protocols (www.fgsc.net/Neurospora/NeurosporaProtocolGuide.htm) unless otherwise stated.

For microscopy, conidia were cultured in liquid VM for up to 4 hr at 30°C using 8-well Nunc Lab-Tek II Chambered Coverglass.

4.2 | *N. crassa* transformation

Electroporation of macroconidia was carried out using the following settings: resistance 600 Ω, voltage 1.5 kV/cm, and capacitance 25 μFd.

4.3 | Heterokaryon purification

N. crassa strains that were obtained as heterokaryons, were purified to homokaryons by standard procedure (www.fgsc.net/Neurospora/NeurosporaProtocolGuide.htm).

4.4 | Plasmids

In order to create pTef1AeqS, aequorin was amplified from pAB19 using the primers AeqS-F and AeqS-R. The vector pCC019 was digested with PacI and EcoRI and the vector gel purified. Aequorin was then amplified with AeqS-IF-Fw and AeqS-IF-Rv to add overlaps homologous to the backbone while maintaining the digestion sites and the vector was assembled using Gibson assembly. Primer sequences are given in supplementary material.

4.5 | IC_{50} values

IC_{50} values were calculated using clear, U bottom polystyrene microtitre plates. PAF 26 was prepared at two concentrations, 35 and 30 μM, and diluted two-fold appropriately in to reach the final experimental

concentrations. Conidia were diluted to a concentration of 1 X 10^6 in 20% liquid VM and 50 µl dispensed into each well. Experimental PAF26 concentrations (µM) were: [17.50][15.00][8.75][7.50][4.38][3.75][2.19][1.88][1.09][0.94][0.55][0]. Final conidial concentration was of 5 × 10^5 in 10% VM. Absorbance measurements were obtained at 610 nm. This wavelength is close to the 595nm at which the relationship between optical density and fungal biomass is linear (Broekaert *et al*., 1990).

4.6 | Calcium measurements

Coelenterazine (#C-7001, www.biosynth.com) was prepared by dissolving in ice cold methanol (MetOH) under a protective atmosphere in complete darkness to a concentration of 10 µg/µl. Stocks were diluted to the working concentration of 3.175 µg in 10 µl MetOH, 74.78 µM.

Conidia were diluted to a concentration of 1 × 10^6 in 10% VM, coelenterazine was added to a final concentration of 2.5 µM. 100 µl of conidial suspension was used per well of a white microtitre plate and the plates incubated at 25°C in the dark for 6 hr. The light output of aequorin was measured by counting the photons emitted by a single well over 1 s, each well in a row of six being measured once every cycle of 7 s. After recording baseline luminescence, a single row was treated with PAF26 and the light output measured over time. Following this the second row was run with 100 µl 3M $CaCl_2$:20% ethanol (EtOH) injected on cycle 8 to immediately discharge all the aequorin.

4.7 | [Ca^{2+}] calculation

The raw relative light units (RLU) were converted to [Ca^{2+}] using the formula: (Bonora *et al*., 2013)

$$\left[Ca^{2+}\right]M=\left(\frac{\left(\frac{L}{L_{max}}\times\lambda\right)^{\frac{1}{n}}+\left(\left(\frac{L}{L_{max}}\times\lambda\right)^{\frac{1}{n}}\times K_{TR}\right)-1}{K_R-\left(\left(\frac{L}{L_{max}}\times\lambda\right)^{\frac{1}{n}}\times K_R\right)}\right).$$

where, L, is the light intensity at sampling time; L_{max}, is the total light emitted at sampling time; K_R, is the constant for calcium bound state (7,230,000); K_{TR}, is the constant for calcium unbound state (120); λ, is the rate constant for aequorin consumption at saturating [Ca^{2+}] (1); n, is the number of Ca^{2+} binding sites (2.99).

In order to calculate L_{max} the total RLU (RLU_{total}) available was calculated from the discharge of aequorin (RLUd) using the trapezoid rule formula, where the total RLUd available at time point t_n equals:

$$RLUd_{t_{n-1}}+\frac{(t_n-t_{n-1})\times(RLUd_{t_n}+RLUd_{t_{n-1}})}{2}$$

and $RLUd_{total}$ is the final value reached. Switching to the experimental data (RLUe), L_{max} was calculated for each time point as:

$$RLUd_{total}-\left(RLUe_{t_{n-1}}+\left(\frac{(t_n-t_{n-1})\times(RLUe_{t_n}+RLUe_{t_{n-1}})}{2}\right)\right).$$

4.8 | Peptides and peptide handling

Peptides were ordered from GenScript (www.genscript.com) at >98% purity. Stock solutions were prepared in 50:50 dimethyl sulfoxide (DMSO):H_2O buffer. Working peptide solutions were prepared in ddH_2O.

4.9 | Microscopy

All microscopy was carried out on a Nikon Eclipse TE2000-E inverted microscope, using a Nikon Plan Apo 60 X 1.2 N.A. DIC H water immersion objective and Nikon G-2A and B-2A filter sets, excitation was provided by a CoolLED illumination system set at 550 nm for use with the G-2A filter or 470 nm for use with the B2-A filter.

Confocal microscopy was carried out using a Leica TCS SP8 equipped with two hybrid GaAsP detectors (HyD) and two photomultiplier tubes (PMT). Excitation was provided using either the Leica tuneable white light laser (450–750 nm), an argon laser (458, 476, 488 and 496 nm) or UV laser (405 nm). Images were captured using LAS X software and the Leica 63 X water immersion objective. All image handling and analysis was carried out using Fiji (fiji.sc/Fiji).

4.10 | Quantification of Ca^{2+} signaling

Fluorescence values were exported from Fiji and analyzed in Excel. Data were normalized using feature scaling. This scales the data to remove irregularities in GCaMP6 expression and photon yield. The function used was: x^I = MIN + (x-min_x)(MAX-MIN)/(max_x-min_x). Where MIN and MAX are the required scale range, x is the original value and x^I is the normalized value. min_x is the minimum value for that data set and max_x is the maximum, max_x was defined as the maximum value from all experiments plus 10 to avoid artificial amplification of noise. The noise was removed using an IF function: =IF(x > y, x, 0) where x is the data point and y is the noise threshold limit. Finally, an IF(AND(x > x_{-1}, x > x_{+1}),1,0) function, where x_{-1} and x_{+1} are the surrounding measurements, quantified each peak in GCamP6 fluorescence.

DATA AVAILABILITY STATEMENT

Data used in this study are available at: http://dx.doi.org/10.17632/sb2r2zsxdz.1.

ORCID

Akira J. T. Alexander https://orcid.org/0000-0003-1601-619X
Alberto Muñoz https://orcid.org/0000-0002-1622-5074
Jose F. Marcos https://orcid.org/0000-0003-3339-2584
Nick D. Read https://orcid.org/0000-0002-2286-2862

REFERENCES

Antebi, A. and Fink, G.R. (1992) The yeast $Ca^{(2+)}$-ATPase homologue, PMR1, is required for normal Golgi function and localizes in a novel Golgi-like distribution. *Molecular Biology of the Cell*, *3*(6), 633–654.

Bagnat, M., Chang, A. and Simons, K. (2001) Plasma membrane proton ATPase Pma1p requires raft association for surface delivery in yeast. *Molecular Biology of the Cell*, *12*(12), 4129–4138.

Bayer, M.J., Reese, C., Buhler, S., Peters, C. and Mayer, A. (2003) Vacuole membrane fusion: V0 functions after trans-SNARE pairing and is coupled to the Ca2+-releasing channel. *The Journal of Cell Biology*, *162*(2), 211–222.

Benito, B., Garciadeblás, B., Pérez-Martín, J. and Rodríguez-Navarro, A. (2009) Growth at high pH and sodium and potassium tolerance in media above the cytoplasmic pH depend on ENA ATPases in *Ustilago maydis*. *Eukaryotic Cell*, *8*(6), 821–829.

Benito, B., Garciadeblas, B. and Rodriguez-Navarro, A. (2000) Molecular cloning of the calcium and sodium ATPases in *Neurospora crassa*. *Molecular Microbiology*, *35*(5), 1079–1088.

Bertl, A. and Slayman, C.L. (1990) Cation-selective channels in the vacuolar membrane of *Saccharomyces*: dependence on calcium, redox state, and voltage. *Proceedings of the National Academy of Sciences of the United States of America*, *87*(20), 7824–7828.

Binder, U., Chu, M., Read, N.D. and Marx, F. (2010) The antifungal activity of the *Penicillium chrysogenum* protein PAF disrupts calcium homeostasis in *Neurospora crassa*. *Eukaryotic Cell*, *9*(9), 1374–1382.

Bongomin, F., Gago, S., Oladele, O.R. and Denning, W.D. (2017) Global and multi-national prevalence of fungal diseases—estimate precision. *Journal of Fungi*, *3*(4), 57.

Bonora, M., Giorgi, C., Bononi, A., Marchi, S., Patergnani, S., Rimessi, A., *et al*. (2013) Subcellular calcium measurements in mammalian cells using jellyfish photoprotein aequorin-based probes. *Nature Protocols*, *8*(11), 2105–2118.

Bormann, J. and Tudzynski, P. (2009) Deletion of Mid1, a putative stretch-activated calcium channel in *Claviceps purpurea*, affects vegetative growth, cell wall synthesis and virulence. *Microbiology*, *155*(12), 3922–3933.

Bowman, B.J., Abreu, S., Margolles-Clark, E., Draskovic, M. and Bowman, E.J. (2011) Role of four calcium transport proteins, encoded by *nca-1*, *nca-2*, *nca-3*, and *cax*, in maintaining intracellular calcium levels in *Neurospora crassa*. *Eukaryotic Cell*, *10*(5), 654–661.

Bowman, B.J., Blasco, F. and Slayman, C.W. (1981) Purification and characterization of the plasma membrane ATPase of *Neurospora crassa*. *Journal of Biological Chemistry*, *256*(23), 12343–12349.

Bowman, B.J., Draskovic, M., Freitag, M. and Bowman, E.J. (2009) Structure and distribution of organelles and cellular location of calcium transporters in *Neurospora crassa*. *Eukaryotic Cell*, *8*(12), 1845–1855.

Brand, A., Shanks, S., Duncan, V.M.S., Yang, M., Mackenzie, K. and Gow, N.A.R. (2007) Hyphal orientation of *Candida albicans* is regulated by a calcium-dependent mechanism. *Current Biology*, *17*(4), 347–352.

Broekaert, W.F., Terras, F.R., Cammue, B.P. and Vanderleyden, J. (1990) An automated quantitative assay for fungal growth inhibition. *FEMS Microbiology Letters*, *69*(1–2), 55–59.

Brown, G.D., Denning, D.W., Gow, N.A.R., Levitz, S.M., Netea, M.G. and White, T.C. (2012) Hidden killers: human fungal infections. *Science Translational Medicine*, *4*(165), 165rv113.

Cavinder, B., Hamam, A., Lew, R.R. and Trail, F. (2011) Mid1, a mechanosensitive calcium ion channel, affects growth, development, and ascospore discharge in the filamentous fungus *Gibberella zeae*. *Eukaryotic Cell*, *10*(6), 832–841.

Coonrod, E.M., Graham, L.A., Carpp, L.N., Carr, T.M., Stirrat, L., Bowers, K., *et al*. (2013) Homotypic vacuole fusion in yeast requires organelle acidification and not the V-ATPase membrane domain. *Developmental Cell*, *27*(4), 462–468.

Courchesne, W.E. (2002) Characterization of a novel, broad-based fungicidal activity for the antiarrhythmic drug amiodarone. *Journal of Pharmacology and Experimental Therapeutics*, *300*(1), 195–199.

Courchesne, W.E. and Ozturk, S. (2002) Amiodarone induces a caffeine-inhibited, MID1-depedent rise in free cytoplasmic calcium in *Saccharomyces cerevisiae*: amiodarone induces a rise in cytoplasmic calcium in yeast. *Molecular Microbiology*, *47*(1), 223–234.

Denis, V. and Cyert, M.S. (2002) Internal Ca^{2+} release in yeast is triggered by hypertonic shock and mediated by a TRP channel homologue. *The Journal of Cell Biology*, *156*(1), 29–34.

Denning, D.W. and Bromley, M.J. (2015) How to bolster the antifungal pipeline. *Science*, *347*(6229), 1414.

Diamond, G., Zasloff, M., Eck, H., Brasseur, M., Maloy, W.L. and Bevins, C.L. (1991) Tracheal antimicrobial peptide, a cysteine-rich peptide from mammalian tracheal mucosa: peptide isolation and cloning of a cDNA. *Proceedings of the National Academy of Sciences of the United States of America*, *88*(9), 3952–3956.

Duncan, V.M.S. and O'Neil, D.A. (2013) Commercialization of antifungal peptides. *Fungal Biology Reviews*, *26*(4), 156–165.

Erdman, S., Lin, L., Malczynski, M. and Snyder, M. (1998) Pheromone-regulated genes required for yeast mating differentiation. *The Journal of Cell Biology*, *140*(3), 461–483.

Gupta, S.S., Ton, V.-K., Beaudry, V., Rulli, S., Cunningham, K. and Rao, R. (2003) Antifungal activity of amiodarone is mediated by disruption of calcium homeostasis. *Journal of Biological Chemistry*, *278*(31), 28831–28839.

Hajdu, D., Huber, A., Czajlik, A., Tóth, L., Kele, Z., Kocsubé, S., *et al*. (2019) Solution structure and novel insights into phylogeny and mode of action of the Neosartorya (*Aspergillus*) fischeri antifungal protein (NFAP). *International Journal of Biological Macromolecules*, *129*, 511–522.

Hallen, H.E. and Trail, F. (2008) The L-type calcium ion channel Cch1 affects ascospore discharge and mycelial growth in the filamentous fungus *Gibberella zeae* (Anamorph *Fusarium graminearum*). *Eukaryotic Cell*, *7*(2), 415–424.

Hamam, A. and Lew, R.R. (2012) Electrical phenotypes of calcium transport mutant strains of a filamentous fungus, *Neurospora crassa*. *Eukaryotic cell*, *11*(5), 694–702.

Huber, A., Hajdu, D., Bratschun-Khan, D., Gáspári, Z., Varbanov, M., Philippot, S., *et al*. (2018) New antimicrobial potential and structural properties of PAFB: a cationic, cysteine-rich protein from *Penicillium chrysogenum* Q176. *Scientific Reports*, *8*(1), 1751.

Iida, H., Nakamura, H., Ono, T., Okumura, M.S. and Anraku, Y. (1994) MID1, a novel *Saccharomyces cerevisiae* gene encoding a plasma membrane protein, is required for Ca2+ influx and mating. *Molecular and Cellular Biology*, *14*(12), 8259–8271.

Kaiserer, L., Oberparleiter, C., Weiler-Görz, R., Burgstaller, W., Leiter, E. and Marx, F. (2003) Characterization of the *Penicillium chrysogenum* antifungal protein PAF. *Archives of Microbiology*, *180*(3), 204–210.

Kanzaki, M. (1999) Molecular identification of a eukaryotic, stretch-activated nonselective cation channel. *Science*, *285*(5429), 882–886.

Kim, S. and Lee, D.G. (2019) Role of calcium in reactive oxygen species-induced apoptosis in *Candida albicans*: an antifungal mechanism of antimicrobial peptide, PMAP-23. *Free Radical Research*, *53*(1), 8–17.

Kohler, J.R., Casadevall, A. and Perfect, J. (2014) The spectrum of fungi that infects humans. *Cold Spring Harbor Perspectives in Medicine*, *5*(1), a019273.

Lapinskas, P.J., Cunningham, K.W., Liu, X.F., Fink, G.R. and Culotta, V.C. (1995) Mutations in PMR1 suppress oxidative damage in yeast cells lacking superoxide dismutase. *Molecular and Cellular Biology*, *15*(3), 1382–1388.

Levina, N.N., Lew, R.R., Hyde, G.J. and Heath, I.B. (1995) The roles of Ca^{2+} and plasma membrane ion channels in hyphal tip growth of *Neurospora crassa*. *Journal of Cell Science*, *108*(Pt 11), 3405–3417.

Lew, R.R., Abbas, Z., Anderca, M.I. and Free, S.J. (2008) Phenotype of a mechanosensitive channel mutant, *mid-1*, in a filamentous fungus, *Neurospora crassa*. *Eukaryotic Cell*, *7*(4), 647–655.

Li, R., Chen, C., Zhang, B., Jing, H., Wang, Z., Wu, C., *et al* (2019) The chromogranin A-derived antifungal peptide CGA-N9 induces apoptosis in *Candida tropicalis*. *Biochemical Journal*, *476*(20), 3069–3080.

Lis, M., Liu, T.T., Barker, K.S., Rogers, P.D. and Bobek, L.A. (2010) Antimicrobial peptide MUC7 12-mer activates the calcium/calcineurin pathway in *Candida albicans*. *FEMS Yeast Research*, *10*(5), 579–586.

Liu, Y., Sitaraman, S. and Chang, A. (2006) Multiple degradation pathways for misfolded mutants of the yeast plasma membrane ATPase, PMA1. *Journal of Biological Chemistry*, *281*(42), 31457–31466.

Locke, E.G., Bonilla, M., Liang, L., Takita, Y. and Cunningham, K.W. (2000) A homolog of voltage-gated Ca^{2+} channels stimulated by depletion of secretory Ca^{2+} in yeast. *Molecular and Cellular Biology*, *20*(18), 6686–6694.

Mahlapuu Margit, Håkansson Joakim, Ringstad Lovisa, Björn Camilla (2016) Antimicrobial Peptides: An Emerging Category of Therapeutic Agents. *Frontiers in Cellular and Infection Microbiology*, *6*, 194. http://dx.doi.org/10.3389/fcimb.2016.00194.

Matejuk, A., Leng, Q., Begum, M.D., Woodle, M.C., Scaria, P., Chou, S.T., *et al*. (2010) Peptide-based antifungal therapies against emerging infections. *Drugs Future*, *35*(3), 197.

Merz, A.J. and Wickner, W.T. (2004) Trans-SNARE interactions elicit Ca^{2+} efflux from the yeast vacuole lumen. *The Journal of Cell Biology*, *164*(2), 195–206.

Muller, E.M., Locke, E.G. and Cunningham, K.W. (2001) Differential regulation of two $Ca^{(2+)}$ influx systems by pheromone signaling in *Saccharomyces cerevisiae*. *Genetics*, *159*(4), 1527–1538.

Muller, E.M., Mackin, N.A., Erdman, S.E. and Cunningham, K.W. (2003) Fig1p facilitates Ca^{2+} influx and cell fusion during mating of *Saccharomyces cerevisiae*. *Journal of Biological Chemistry*, *278*(40), 38461–38469.

Muñoz, A., Gandía, M., Harries, E., Carmona, L., Read, N.D. and Marcos, J.F. (2013a) Understanding the mechanism of action of cell-penetrating antifungal peptides using the rationally designed hexapeptide PAF26 as a model. *Fungal Biology Reviews*, *26*(4), 146–155.

Muñoz, A., Harries, E., Contreras-Valenzuela, A., Carmona, L., Read, N.D. and Marcos, J.F. (2013b) Two functional motifs define the interaction, internalization and toxicity of the cell-penetrating antifungal peptide PAF26 on fungal cells. *PLoS One*, *8*(1), e54813.

Munoz, A., Lopez-Garcia, B. and Marcos, J.F. (2006) Studies on the mode of action of the antifungal hexapeptide PAF26. *Antimicrobial Agents and Chemotherapy*, *50*(11), 3847–3855.

Muñoz, A., Marcos, J.F. and Read, N.D. (2012) Concentration-dependent mechanisms of cell penetration and killing by the de novo designed antifungal hexapeptide PAF26: uptake mechanisms of the antifungal peptide PAF26. *Molecular Microbiology*, *85*(1), 89–106.

Nicola, A.M., Albuquerque, P., Paes, H.C., Fernandes, L., Costa, F.F., Kioshima, E.S., *et al*. (2019) Antifungal drugs: new insights in research & development. *Pharmacology & Therapeutics*, *195*, 21–38.

Paidhungat, M. and Garrett, S. (1997) A homolog of mammalian, voltage-gated calcium channels mediates yeast pheromone-stimulated Ca2+ uptake and exacerbates the cdc1(Ts) growth defect. *Molecular and Cellular Biology*, *17*(11), 6339–6347.

Palmer, C.P., Zhou, X.L., Lin, J., Loukin, S.H., Kung, C. and Saimi, Y. (2001) A TRP homolog in *Saccharomyces cerevisiae* forms an intracellular $Ca^{(2+)}$-permeable channel in the yeast vacuolar membrane. *Proceedings of the National Academy of Sciences of the United States of America*, *98*(14), 7801–7805.

Parisi, K., Doyle, S.R., Lee, E., Lowe, R.G.T., van der Weerden, N.L., Anderson, M.A., *et al*. (2019) Screening the *Saccharomyces cerevisiae* nonessential gene deletion library reveals diverse mechanisms of action for antifungal plant defensins. *Antimicrobial Agents and Chemotherapy*, *63*(11), e01097-1019.

Peters, C. and Mayer, A. (1998) Ca^{2+}/calmodulin signals the completion of docking and triggers a late step of vacuole fusion. *Nature*, *396*(6711), 575–580.

Rautenbach, M., Troskie, A.M. and Vosloo, J.A. (2016) Antifungal peptides: to be or not to be membrane active. *Biochimie*, *130*, 132–145.

Wada, Y., Ohsumi, Y., Tanifuji, M., Kasai, M. and Anraku, Y. (1987) Vacuolar ion channel of the yeast, *Saccharomyces cerevisiae*. *Journal of Biological Chemistry*, *262*(36), 17260–17263.

Yang, X. and Sachs, F. (1989) Block of stretch-activated ion channels in *Xenopus* oocytes by gadolinium and calcium ions. *Science*, *243*(4894), 1068–1071.

Zelter, A., Bencina, M., Bowman, B.J., Yarden, O. and Read, N.D. (2004) A comparative genomic analysis of the calcium signaling machinery in *Neurospora crassa*, *Magnaporthe grisea*, and *Saccharomyces cerevisiae*. *Fungal Genetics and Biology*, *41*(9), 827–841.

Zhou, X.L., Batiza, A.F., Loukin, S.H., Palmer, C.P., Kung, C. and Saimi, Y. (2003) The transient receptor potential channel on the yeast vacuole is mechanosensitive. *Proceedings of the National Academy of Sciences of the United States of America*, *100*(12), 7105–7110.

Mahlapuu, M., Håkansson, J., Ringstad, L., & Björn, C. (2016). Antimicrobial peptides: an emerging category of therapeutic agents. *Frontiers in cellular and infection microbiology*, *6*, 194.

SUPPORTING INFORMATION

Additional supporting information may be found online in the Supporting Information section.

How to cite this article: Alexander AJT, Munoz A, Marcos JF, Read ND. Calcium homeostasis plays important roles in the internalization and activities of the small synthetic antifungal peptide PAF26. *Mol Microbiol*. 2020;114:521–535. https://doi.org/10.1111/mmi.14532